Research Square

Preprints are preliminary reports that have not undergone peer review.
They should not be considered conclusive, used to inform clinical practice,
or referenced by the media as validated information.

A Direct–Indirect Homotopic Approach for Fuel-Optimal Low-Thrust DRO-to-NRHO Transfer in Cislunar Space

Hongxiang Luo
Zhongtao Zhang
Yasheng Zhang
zhangyspublic@163.com

Xuefeng Tao
Wenhua Cheng
Yuan Zeng

Article

Keywords: low-thrust, CR3BP, pseudospectral method, indirect method, homotopy, fuel-optimal

Posted Date: August 5th, 2026

DOI: https://doi.org/10.21203/rs.3.rs-10488764/v1

License: This work is licensed under a Creative Commons Attribution 4.0 International License.
Read Full License

Additional Declarations: No competing interests reported.

A Direct–Indirect Homotopic Approach for Fuel-Optimal Low-Thrust DRO-to-NRHO Transfer in Cislunar Space

Hongxiang Luo[1], Zhongtao Zhang[1], Yasheng Zhang[1*], Xuefeng Tao[1], Wenhua Cheng[1], Yuan Zeng[1]

[1*]Space Engineering University, Beijing, China.

*Corresponding author(s). E-mail(s): zhangyspublic@163.com;
Contributing authors: lhx0919@hgd.edu.cn;

Abstract

Fuel-optimal low-thrust transfer between cislunar periodic orbits gives rise to a sensitive indirect optimal-control problem because the optimal throttle approaches a bang-bang structure and the resulting two-point boundary-value problem depends strongly on the initial costates. This paper studies a fixed-time transfer from a distant retrograde orbit to a near-rectilinear halo orbit in the Earth–Moon circular restricted three-body problem. A direct–indirect homotopic procedure is developed for this transfer. A smooth energy-optimal auxiliary problem is first solved by a Radau pseudospectral transcription in GPOPS-II, and the recovered costate estimate initializes an indirect shooting formulation. The shooting problem is then continued from the energy-optimal index toward the fuel-optimal index through a homotopy parameter. A representative 5-day transfer demonstrates costate reconstruction, homotopic costate evolution, combined throttle and fuel-consumption histories, and the final transfer trajectory. A computed all-phase fuel-consumption map identifies the most fuel-saving phase pair within the sampled grid.

Keywords: low-thrust; CR3BP; pseudospectral method; indirect method; homotopy; fuel-optimal

1 Introduction

Near-rectilinear halo orbits are operationally relevant cislunar destinations, as illustrated by Gateway and CAPSTONE [1, 2]. Distant retrograde orbits also provide useful staging-orbit options [3]. Low-thrust transfer between these families is attractive because it can exploit high specific impulse, but the Earth–Moon circular restricted three-body problem (CR3BP) is nonlinear and the endpoints lie on periodic orbits. For prescribed flight times, minimum-fuel solutions generally approach bang-bang thrusting, so the indirect two-point boundary-value problem is highly sensitive to its initial costates [6].

Direct transcription provides feasible state and control histories, whereas indirect methods expose the switching structure through the Pontryagin minimum principle [5]. These complementary approaches remain central to low-thrust trajectory design [11, 12]. Their combination is particularly useful when a smooth direct solution can supply a costate seed for shooting. Pseudospectral multiplier mappings provide this link [7, 18]. Related cislunar studies have demonstrated direct trajectory construction [15, 20] and homotopic regularization [19].

This paper formulates a fixed-time, free-final-mass DRO-to-NRHO transfer in the Earth–Moon CR3BP and applies a direct–indirect homotopic solution chain. A Radau/GPOPS-II energy-optimal auxiliary problem supplies a costate estimate, after which indirect continuation recovers the fuel-oriented control. This initialization strategy is consistent with recent co-state-initialization efforts [16]. A representative 5-day transfer verifies the costate initialization, continuation behavior, fuel-consumption history, and final trajectory. The final phase map reports the best phase pair within the computed grid.

The remainder of the paper is organized as follows. Section 2 presents the dynamical model and indirect optimal-control framework. Section 3 introduces the Radau pseudospectral framework used for costate initialization. Section 4 gives the algorithm flowchart and numerical procedure. Section 5 presents the simulation results, and Section 6 concludes the paper.

2 Dynamical Modeling and Indirect Framework

This section defines the continuous-time transfer problem and the indirect optimality system used for shooting. The notation follows the Earth–Moon CR3BP convention [4, 14] and is kept consistent across the continuous and discrete formulations. In the indirect formulation, ρ denotes throttle, $\boldsymbol{\alpha}$ denotes thrust direction, and ε denotes the homotopy parameter.

2.1 Low-Thrust Dynamics in the Earth–Moon CR3BP

The DRO-to-NRHO transfer is modeled in the Earth–Moon CR3BP in the synodic rotating frame [4]. The nondimensional mass parameter is

$$\mu = \frac{m_M}{m_E + m_M}, \tag{1}$$

where m_E and m_M are the masses of the Earth and Moon. The spacecraft state is

$$\boldsymbol{x} = \begin{bmatrix} \boldsymbol{r} \\ \boldsymbol{v} \\ m \end{bmatrix} \in \mathbb{R}^7, \qquad \boldsymbol{r} = [x, y, z]^\mathsf{T}, \qquad \boldsymbol{v} = [v_x, v_y, v_z]^\mathsf{T}, \tag{2}$$

where m is the spacecraft mass. In the indirect formulation, the thrust vector is parameterized as

$$\boldsymbol{T} = T_{\max}\rho\boldsymbol{\alpha}, \qquad 0 \le \rho \le 1, \qquad \|\boldsymbol{\alpha}\| = 1, \tag{3}$$

with $T_{\max}$ the maximum thrust, ρ the throttle, and $\boldsymbol{\alpha}$ the thrust direction. The normalized low-thrust dynamics are

$$\dot{\boldsymbol{r}} = \boldsymbol{v}, \tag{4a}$$

$$\dot{\boldsymbol{v}} = \boldsymbol{g}(\boldsymbol{r}) + \boldsymbol{h}(\boldsymbol{v}) + \frac{T_{\max}}{m}\rho\boldsymbol{\alpha}, \tag{4b}$$

$$\dot{m} = -\frac{T_{\max}}{I_{\mathrm{sp}} g_0}\rho, \tag{4c}$$

where I_{sp} is the specific impulse and g_0 is the standard gravitational acceleration. The position-dependent CR3BP term is

$$\boldsymbol{g}(\boldsymbol{r}) = \begin{bmatrix} x - \dfrac{(1-\mu)(x+\mu)}{r_1^3} - \dfrac{\mu(x+\mu-1)}{r_2^3} \\ y - \dfrac{(1-\mu)y}{r_1^3} - \dfrac{\mu y}{r_2^3} \\ -\dfrac{(1-\mu)z}{r_1^3} - \dfrac{\mu z}{r_2^3} \end{bmatrix}, \tag{5}$$

and the velocity-dependent rotating-frame term is

$$\boldsymbol{h}(\boldsymbol{v}) = \begin{bmatrix} 2v_y \\ -2v_x \\ 0 \end{bmatrix}. \tag{6}$$

The distances from the spacecraft to the two primaries are

$$r_1 = \sqrt{(x+\mu)^2 + y^2 + z^2}, \qquad r_2 = \sqrt{(x+\mu-1)^2 + y^2 + z^2}. \tag{7}$$

Equations (4)–(7) are the continuous dynamics used in the direct and indirect stages.

2.2 Boundary Conditions for the DRO-to-NRHO Transfer

Let $\boldsymbol{x}_{\mathrm{D}}(\tau_{\mathrm{D}})$ be a state on the departure DRO and $\boldsymbol{x}_{\mathrm{N}}(\tau_{\mathrm{N}})$ be a state on the target NRHO, where τ_{D} and τ_{N} denote orbit phase parameters. This boundary description

is consistent with phase-dependent periodic-orbit transfer formulations in the Earth–Moon system [21]. The general phase-to-phase transfer can be written as

$$\boldsymbol{x}(t_0) = \boldsymbol{x}_{\mathrm{D}}(\tau_{\mathrm{D}}), \qquad \boldsymbol{x}(t_{\mathrm{f}}) = \boldsymbol{x}_{\mathrm{N}}(\tau_{\mathrm{N}}). \tag{8}$$

The representative transfer studied here uses one prescribed departure state and one prescribed arrival state. The initial boundary conditions are

$$\boldsymbol{r}(t_0) = \boldsymbol{r}_0, \qquad \boldsymbol{v}(t_0) = \boldsymbol{v}_0, \qquad m(t_0) = m_0, \tag{9a}$$

and the terminal rendezvous conditions are

$$\boldsymbol{r}(t_{\mathrm{f}}) = \boldsymbol{r}_{\mathrm{f}}, \qquad \boldsymbol{v}(t_{\mathrm{f}}) = \boldsymbol{v}_{\mathrm{f}}. \tag{9b}$$

The final mass is free, whereas the transfer time is prescribed; the result is a fixed-time rendezvous problem with free terminal mass.

2.3 Fuel-Optimal, Energy-Optimal, and Homotopic Performance Indices

For a prescribed transfer time, minimizing propellant consumption is equivalent to minimizing the throttle integral, a standard performance index in low-thrust minimum-fuel optimal control [9, 10]:

$$J_{\mathrm{F}} = \frac{T_{\max}}{I_{\mathrm{sp}} g_0} \int_{t_0}^{t_{\mathrm{f}}} \rho(t)\, \mathrm{d}t = m_0 - m(t_{\mathrm{f}}). \tag{10}$$

The energy-optimal auxiliary index is defined as

$$J_{\mathrm{E}} = \frac{T_{\max}}{I_{\mathrm{sp}} g_0} \int_{t_0}^{t_{\mathrm{f}}} \rho^2(t)\, \mathrm{d}t. \tag{11}$$

A homotopic family connects these two objectives:

$$J_\varepsilon = \frac{T_{\max}}{I_{\mathrm{sp}} g_0} \int_{t_0}^{t_{\mathrm{f}}} \left[(1-\varepsilon)\rho + \varepsilon \rho^2\right]\, \mathrm{d}t, \qquad \varepsilon \in [0,1]. \tag{12}$$

The case $\varepsilon = 1$ gives the smooth energy-optimal problem, and $\varepsilon = 0$ gives the fuel-optimal problem. The continuation in ε is the basis of the indirect homotopy used later.

2.4 Hamiltonian, Switching Law, and Costate Equations

The costate vector is

$$\boldsymbol{\lambda} = \begin{bmatrix} \boldsymbol{\lambda}_r \\ \boldsymbol{\lambda}_v \\ \lambda_m \end{bmatrix} \in \mathbb{R}^7. \tag{13}$$

For the homotopic index in Equation (12), the Hamiltonian is obtained from the PMP formulation of low-thrust optimal control [5, 13]:

$$\begin{aligned}\mathcal{H} = \boldsymbol{\lambda}_r^{\mathsf{T}}\boldsymbol{v} + \boldsymbol{\lambda}_v^{\mathsf{T}}\left(\boldsymbol{g}(\boldsymbol{r}) + \boldsymbol{h}(\boldsymbol{v}) + \frac{T_{\max}}{m}\rho\boldsymbol{\alpha}\right) - \lambda_m\frac{T_{\max}}{I_{\mathrm{sp}}g_0}\rho \\ + \frac{T_{\max}}{I_{\mathrm{sp}}g_0}\left[(1-\varepsilon)\rho + \varepsilon\rho^2\right].\end{aligned} \tag{14}$$

Minimization of $\mathcal{H}$ with respect to the thrust direction gives

$$\boldsymbol{\alpha}^* = -\frac{\boldsymbol{\lambda}_v}{\|\boldsymbol{\lambda}_v\|}. \tag{15}$$

The switching function is defined by

$$S = 1 - \lambda_m - \frac{I_{\mathrm{sp}}g_0}{m}\|\boldsymbol{\lambda}_v\|. \tag{16}$$

For $0 < \varepsilon \leq 1$, the throttle law is

$$\rho^* = \begin{cases} 0, & S > \varepsilon, \\ \dfrac{\varepsilon - S}{2\varepsilon}, & |S| \leq \varepsilon, \\ 1, & S < -\varepsilon. \end{cases} \tag{17}$$

As ε decreases, the transition layer in Equation (17) becomes narrower and the bang-bang fuel-optimal structure is approached.

Let

$$\mathbf{G}(\boldsymbol{r}) = \frac{\partial \boldsymbol{g}}{\partial \boldsymbol{r}}, \qquad \mathbf{C} = \frac{\partial \boldsymbol{h}}{\partial \boldsymbol{v}} = \begin{bmatrix} 0 & 2 & 0 \\ -2 & 0 & 0 \\ 0 & 0 & 0 \end{bmatrix}. \tag{18}$$

The costate dynamics are

$$\dot{\boldsymbol{\lambda}}_r = -\mathbf{G}^{\mathsf{T}}(\boldsymbol{r})\boldsymbol{\lambda}_v, \tag{19a}$$

$$\dot{\boldsymbol{\lambda}}_v = -\boldsymbol{\lambda}_r - \mathbf{C}^{\mathsf{T}}\boldsymbol{\lambda}_v, \tag{19b}$$

$$\dot{\lambda}_m = -\frac{T_{\max}}{m^2}\rho^*\|\boldsymbol{\lambda}_v\|. \tag{19c}$$

Since the terminal mass is free, the corresponding transversality condition is

$$\lambda_m(t_{\mathrm{f}}) = 0. \tag{20}$$

The indirect problem is therefore a TPBVP. The initial costate $\boldsymbol{\lambda}(t_0)$ is determined by the residual

$$\boldsymbol{Z}(\boldsymbol{\lambda}(t_0)) = \begin{bmatrix} \boldsymbol{r}(t_{\mathrm{f}}) - \boldsymbol{r}_{\mathrm{f}} \\ \boldsymbol{v}(t_{\mathrm{f}}) - \boldsymbol{v}_{\mathrm{f}} \\ \lambda_m(t_{\mathrm{f}}) \end{bmatrix} = \mathbf{0}. \tag{21}$$

The accuracy of the initial costate strongly affects shooting convergence. The pseudospectral stage in Section 3 supplies the costate estimate used to initialize this TPBVP.

3 Pseudospectral Framework for Costate Initialization

The indirect formulation in Section 2 requires an initial costate estimate. This estimate is obtained from a smooth direct auxiliary problem. The direct stage uses a Radau pseudospectral transcription of the energy-optimal problem and passes the recovered costate information to the indirect homotopy, following the costate-recovery rationale of pseudospectral optimal-control methods [8].

3.1 Radau Transcription of the Energy-Optimal Problem

The energy-optimal problem in Equation (11) is used for the direct stage. The physical time interval is mapped onto the standard domain by

$$s = \frac{2t - t_\mathrm{f} - t_0}{t_\mathrm{f} - t_0}, \qquad t = \frac{t_\mathrm{f} + t_0}{2} + \frac{t_\mathrm{f} - t_0}{2} s, \qquad s \in [-1, 1]. \tag{22}$$

The direct-stage control is the thrust vector

$$\boldsymbol{\tau}(t) = \begin{bmatrix} \tau_x & \tau_y & \tau_z \end{bmatrix}^\mathsf{T}, \qquad \|\boldsymbol{\tau}\| \le T_\mathrm{max}. \tag{23}$$

The direct dynamics are

$$\dot{\boldsymbol{r}} = \boldsymbol{v}, \tag{24a}$$

$$\dot{\boldsymbol{v}} = \boldsymbol{g}(\boldsymbol{r}) + \boldsymbol{h}(\boldsymbol{v}) + \frac{\boldsymbol{\tau}}{m}, \tag{24b}$$

$$\dot{m} = -\frac{\|\boldsymbol{\tau}\|}{I_\mathrm{sp} g_0}. \tag{24c}$$

Let $s_1, \ldots, s_N$ denote the Legendre–Gauss–Radau collocation points and let $s_{N+1} = 1$ be the terminal point. The state approximation is expressed with Lagrange basis polynomials as

$$\boldsymbol{x}(s) \approx \boldsymbol{X}(s) = \sum_{i=1}^{N+1} L_i(s) \boldsymbol{X}_i. \tag{25}$$

At each collocation point,

$$\left.\frac{\mathrm{d}\boldsymbol{X}}{\mathrm{d}s}\right|_{s=s_k} \approx \sum_{i=1}^{N+1} D_{ki} \boldsymbol{X}_i, \qquad k = 1, \ldots, N, \tag{26}$$

where $D_{ki} = \left.\dfrac{\mathrm{d}L_i}{\mathrm{d}s}\right|_{s=s_k}$. The collocation constraints are

$$\sum_{i=1}^{N+1} D_{ki}\boldsymbol{X}_i - \frac{t_\mathrm{f}-t_0}{2}\boldsymbol{f}_\mathrm{d}(\boldsymbol{X}_k,\boldsymbol{\tau}_k) = \boldsymbol{0}, \qquad k = 1,\ldots,N. \tag{27}$$

The boundary constraints are

$$\boldsymbol{X}_1 = \begin{bmatrix}\boldsymbol{r}_0\\ \boldsymbol{v}_0\\ m_0\end{bmatrix}, \qquad \boldsymbol{r}_{N+1} = \boldsymbol{r}_\mathrm{f}, \qquad \boldsymbol{v}_{N+1} = \boldsymbol{v}_\mathrm{f}, \tag{28}$$

with free terminal mass. The discretized energy objective is

$$J_\mathrm{E}^N = \frac{t_\mathrm{f}-t_0}{2I_\mathrm{sp}g_0T_\mathrm{max}}\sum_{k=1}^{N} w_k\|\boldsymbol{\tau}_k\|^2, \tag{29}$$

and the thrust magnitude is constrained by

$$\|\boldsymbol{\tau}_k\|^2 - T_\mathrm{max}^2 \le 0, \qquad k = 1,\ldots,N. \tag{30}$$

Equations (27)–(30) define the finite-dimensional nonlinear programming problem solved in the direct stage.

3.2 NLP Multipliers and Costate Mapping

The costate estimate is obtained from the multipliers of the direct transcription. Let $\boldsymbol{K}_k$ be the Lagrange multipliers associated with the collocation constraints and let w_k be the quadrature weights. The discrete KKT conditions approximate the continuous first-order necessary conditions, and the costate at the collocation points is estimated through the pseudospectral covector-mapping relation [7] by

$$\widehat{\boldsymbol{\lambda}}_k = \frac{\boldsymbol{K}_k}{w_k}, \qquad k = 1,\ldots,N. \tag{31}$$

The terminal costate is reconstructed as

$$\widehat{\boldsymbol{\lambda}}_{N+1} = D_{N+1}^\mathsf{T}\boldsymbol{K}. \tag{32}$$

This mapping provides the theoretical link between the pseudospectral direct solution and the indirect shooting problem. The costate estimate reconstructed from the direct transcription is used as the initial adjoint seed for homotopy continuation.

3.3 hp-Adaptive Radau Mesh Treatment

The direct stage uses a multi-interval Radau framework with hp-adaptive mesh refinement [8]. The h-refinement changes the number of mesh intervals, while the p-refinement changes the polynomial degree in each interval. This mesh strategy improves the approximation of the smooth energy-optimal solution and therefore improves the quality of the costate estimate passed to the indirect stage.

4 Algorithm Flow and Numerical Procedure

4.1 Overall Workflow

Sections 2 and 3 define the target problem and the pseudospectral initialization framework. The numerical procedure first solves the pseudospectral problem and then performs the indirect homotopy. Figure 1 summarizes the workflow.

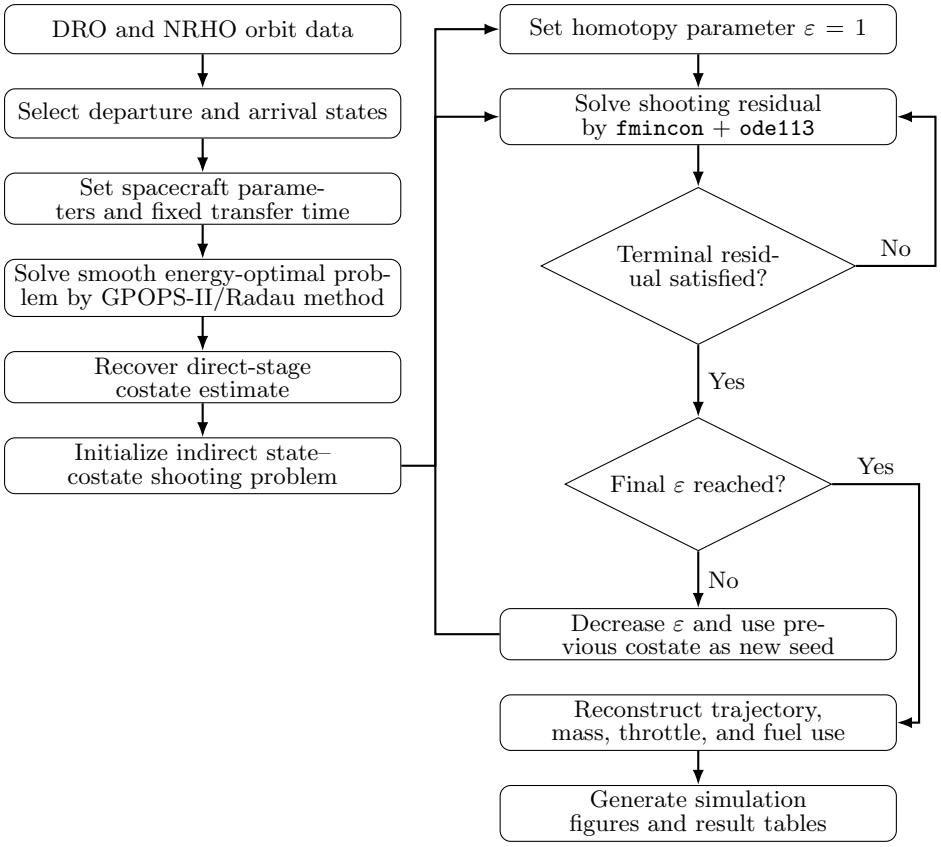


Fig. 1 Flowchart of the direct–indirect homotopic solution procedure.

4.2 Homotopy Continuation Sequence

The homotopy parameter is decreased gradually from the smooth energy-optimal end to a small positive value close to the fuel-optimal limit:

$$1 = \varepsilon_0 > \varepsilon_1 > \cdots > \varepsilon_K, \qquad 0 < \varepsilon_K \ll 1. \tag{33}$$

At each value of ε, the seven initial costates are optimized to satisfy the shooting residual in Equation (21). The converged costates from one step initialize the next step. This continuation strategy moves the solution from the smooth energy-optimal problem toward the fuel-oriented limit without a direct jump to the nearly bang-bang case.

4.3 Numerical Solution Settings

The direct energy-optimal problem is solved in GPOPS-II with SNOPT under a Radau pseudospectral transcription. The indirect shooting problem is solved with `fmincon`, and the coupled state–costate equations are integrated with `ode113`. The terminal residual contains the terminal position error, terminal velocity error, and terminal mass-costate condition. Position and velocity residuals are nondimensionalized by the characteristic distance and velocity units to improve numerical conditioning.

The reported quantities are the transfer trajectory, mass history, throttle or thrust magnitude, costate evolution, switching behavior, fuel consumption, and terminal residuals. These quantities form the basis of the simulation figures in Section 5.

5 Simulation Results

5.1 Numerical Setup and Boundary States

The procedure is evaluated on a fixed-time DRO-to-NRHO transfer in the Earth–Moon CR3BP. The spacecraft initial mass is 500 kg, the maximum thrust is 0.3 N, and the specific impulse is 1000 s. The transfer duration is fixed at 5 days. Unless physical units are stated explicitly, state variables in this section are expressed in the nondimensional synodic CR3BP frame. The Earth–Moon distance unit is 384400 km.

The departure and arrival states are selected on the propagated DRO and NRHO, respectively. The departure state is $\boldsymbol{r}_0 = [1.1780, 0, 0]^\mathsf{T}$, with $\boldsymbol{v}_0 = [0, -0.4966, 0]^\mathsf{T}$. The terminal rendezvous state is $\boldsymbol{r}_\mathrm{f} = [1.0354, 0, -0.1899]^\mathsf{T}$, with $\boldsymbol{v}_\mathrm{f} = [0, -0.1307, 0]^\mathsf{T}$. The propagated departure DRO and target NRHO have orbital periods of 13.9337 days and 7.3395 days. These states define the fixed endpoints for the direct energy-optimal stage and the subsequent indirect homotopy. Table 1 summarizes the main numerical settings.

Table 1 Numerical settings for the representative DRO-to-NRHO transfer.

Quantity	Value
Initial mass	500 kg
Maximum thrust	0.3 N
Specific impulse	1000 s
Transfer time	5 days
Distance unit	384400 km
Pseudospectral discretization	40 nodes

5.2 Energy-Optimal Costate Reconstruction

The computation starts with a smooth energy-optimal auxiliary problem. The initial guess for the direct transcription is sampled from a continuous transfer connecting the prescribed endpoints, and the thrust bound is set to $T_{\max} = 0.3$ N. The Radau pseudospectral transcription uses 40 discretization nodes. After the nonlinear programming problem is solved, the multipliers associated with the collocation constraints are mapped to continuous costates. Figure 2 shows the reconstructed energy-optimal costates $\boldsymbol{\lambda} = [\boldsymbol{\lambda}_r^{\mathsf{T}}, \boldsymbol{\lambda}_v^{\mathsf{T}}, \lambda_m]^{\mathsf{T}}$ over the 5-day transfer. The star markers denote costates estimated from pseudospectral multipliers, and the solid curves denote the continuous costate histories obtained from the shooting formulation. The close agreement is important: it indicates that the direct-stage multipliers provide a viable initialization for the indirect stage, while the terminal mass costate approaches the transversality condition $\lambda_m(t_{\mathrm{f}}) = 0$.

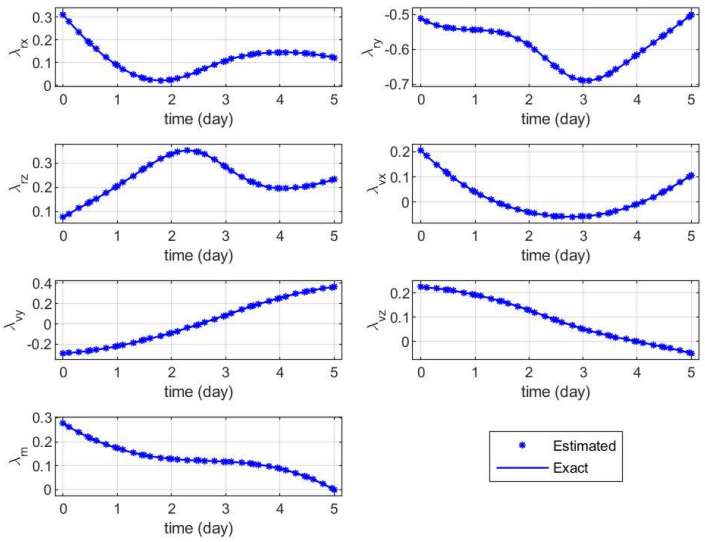


Fig. 2 Costate reconstruction for the energy-optimal DRO-to-NRHO transfer.

5.3 Initial-Costate Continuation

The costates estimated from the energy-optimal direct solution initialize the indirect shooting equations. During continuation, the homotopy parameter is reduced from the energy-optimal side toward the fuel-oriented limit, and the converged costate vector at each step seeds the next step. Figure 3 shows the resulting evolution of the initial costates $\boldsymbol{\lambda}(t_0)$. Each curve records one component of $\boldsymbol{\lambda}(t_0)$ as the homotopy parameter decreases, making visible how the smooth direct-stage initialization is transported toward the fuel-oriented indirect solution.

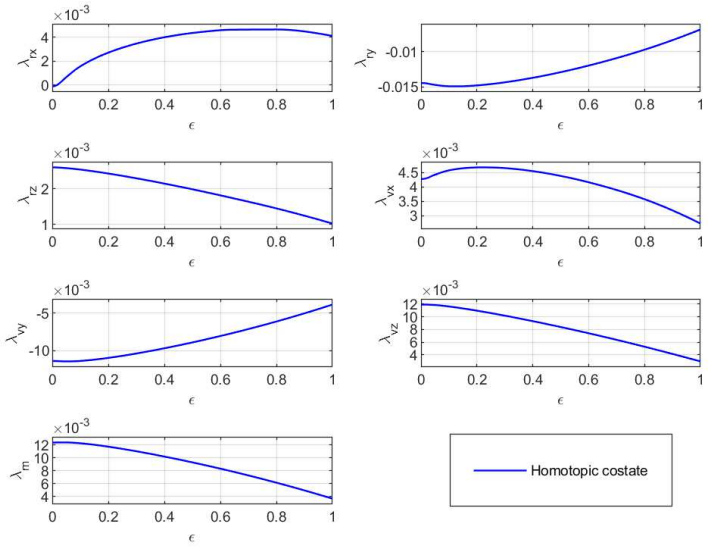


Fig. 3 Evolution of the initial costates during homotopy continuation.

Table 2 compares the energy-optimal costate estimate with the accurate fuel-optimal initial costates. It lists all seven initial components, including the position, velocity, and mass costates used in the shooting equations.

Table 2 Initial costates used in the direct–indirect continuation.

Costate component	Estimated initial costates (energy-optimal)	Accurate initial costates (fuel-optimal)
$\lambda_{r_x}(t_0)$	0.1940	-0.0001
$\lambda_{r_y}(t_0)$	-0.5367	-0.0145
$\lambda_{r_z}(t_0)$	0.1330	0.0026
$\lambda_{v_x}(t_0)$	0.1200	0.0043
$\lambda_{v_y}(t_0)$	-0.2669	-0.0114
$\lambda_{v_z}(t_0)$	0.2134	0.0119
$\lambda_m(t_0)$	0.2207	0.0124

5.4 Homotopic Throttle Evolution and Fuel-Optimal Transfer

Figure 4 combines the control and fuel histories at representative homotopy values. In panel (a), the throttle coefficient ρ evolves from the smooth energy-optimal case to the near fuel-optimal case. At small ε, it is concentrated near its bounds, with short full-thrust arcs and a long coast interval, as expected for a bounded-thrust minimum-fuel transfer [17]. The switching-related thrust behavior provides a numerical check of Equation (17). Panel (b) shows the corresponding fuel-consumption histories: intermediate solutions are dashed, while the final solution is the solid curve. Together, the panels show how homotopy sharpens the switching structure and reshapes the mass-consumption history, consistent with recent smoothing-homotopy studies [22].

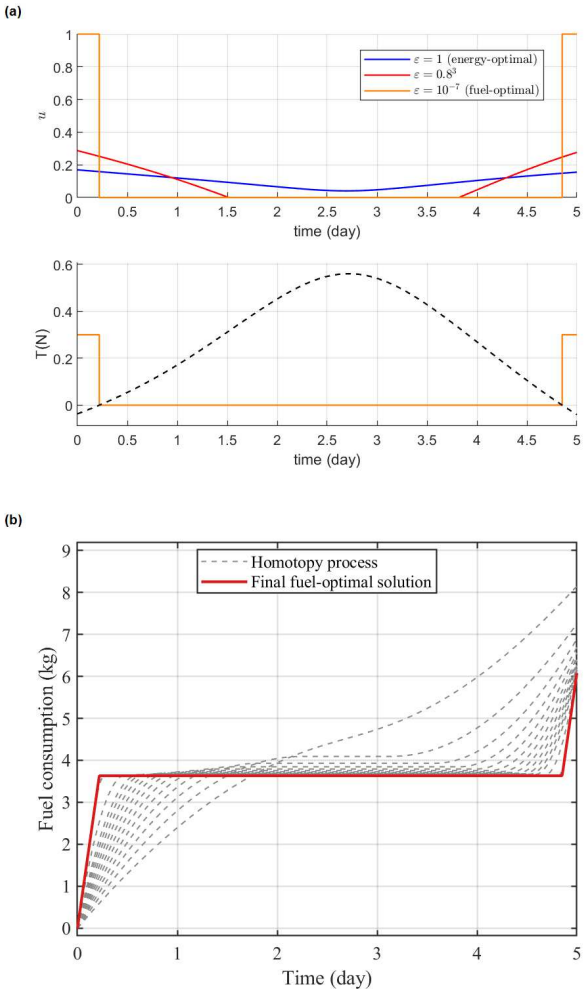


Fig. 4 Homotopic evolution of throttle and fuel consumption. (a) Throttle coefficient and switching-related thrust behavior during continuation. (b) Fuel-consumption histories for the same continuation sequence.

Figure 5 presents the fuel-optimal transfer trajectory obtained after homotopy continuation. Together with the control and fuel histories in Figure 4, this trajectory gives the fuel-oriented indirect solution for the prescribed 5-day endpoint pair.

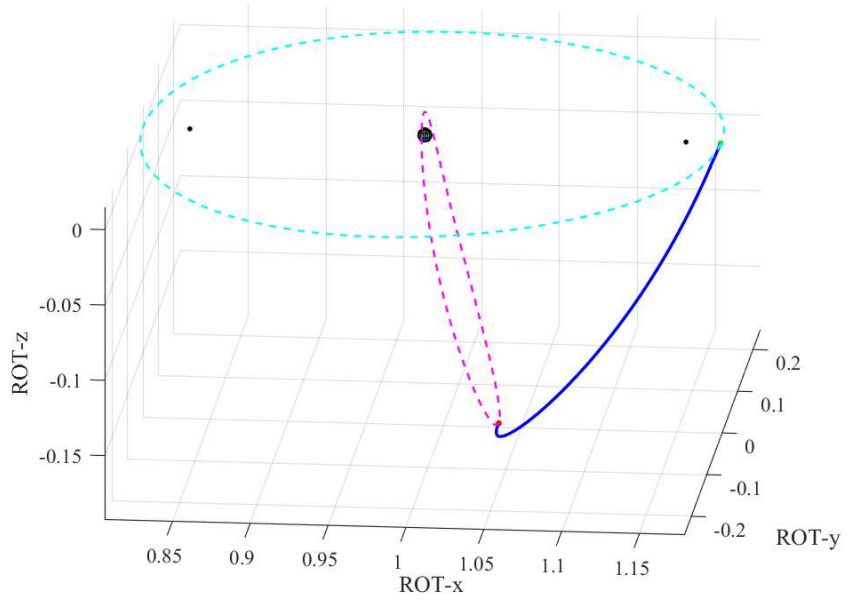


Fig. 5 Fuel-optimal DRO-to-NRHO transfer trajectory in the rotating CR3BP frame.

5.5 All-Phase Fuel-Consumption Map

Figure 6 presents the computed all-phase fuel-consumption map. The horizontal and vertical axes denote the normalized departure phase on the DRO and the normalized arrival phase on the NRHO, respectively, while the color value denotes the fuel consumption of the corresponding transfer. Within the computed phase grid, the minimum-fuel transfer departs from the DRO phase represented by $\boldsymbol{r}_{\mathrm{D}}^{\star} = [0.9239, 0.2349, 0]^{\mathsf{T}}$ and $\boldsymbol{v}_{\mathrm{D}}^{\star} = [0.3241, 0.1477, 0]^{\mathsf{T}}$, and arrives at the NRHO phase represented by $\boldsymbol{r}_{\mathrm{N}}^{\star} = [1.0353, -0.0054, -0.1896]^{\mathsf{T}}$ and $\boldsymbol{v}_{\mathrm{N}}^{\star} = [-0.0067, -0.1303, 0.0191]^{\mathsf{T}}$. These state vectors specify the orbit parameters of the most fuel-saving phase pair identified in the map. The minimum fuel consumption associated with this phase pair is 4.343 kg.

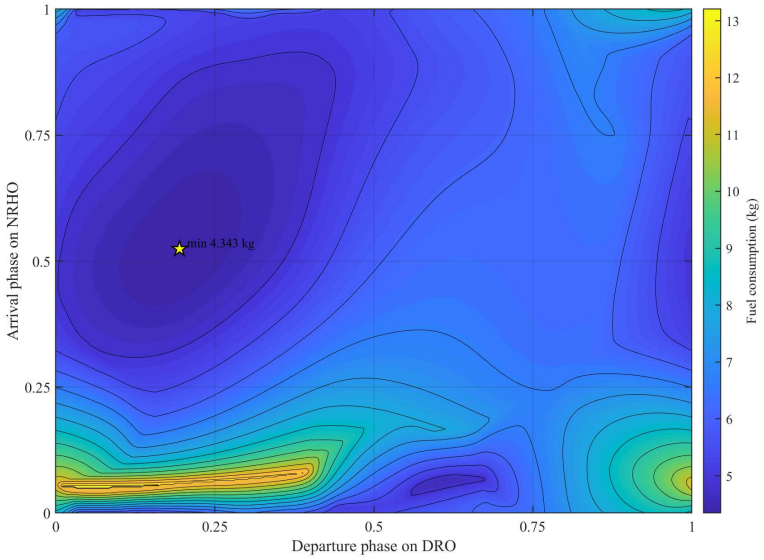


Fig. 6 All-phase fuel-consumption map for DRO-to-NRHO transfers.

6 Conclusion

This paper formulated a fixed-time fuel-optimal low-thrust transfer from a DRO to an NRHO in the Earth–Moon CR3BP and developed a direct–indirect homotopic solution procedure for the representative transfer. The continuous dynamics and indirect framework define the fuel-optimal TPBVP, while the Radau pseudospectral energy-optimal problem provides a practical costate initialization for the indirect homotopy.

The representative 5-day transfer supports the workflow through costate reconstruction, homotopic costate evolution, combined throttle and fuel-consumption histories, and the final transfer trajectory. The approach is applicable to fixed-time, phase-specified transfers between cislunar periodic orbits when a smooth direct solution is available but indirect shooting lacks reliable initial costates. Its main advantage is the combination of direct pseudospectral robustness for initialization with the physical interpretability and bang-bang control recovery of the indirect PMP formulation. Future work will extend the phase-map analysis through higher-fidelity validation of selected phase pairs, variable transfer times, and models including higher-fidelity dynamics and operational constraints.

Acknowledgements

The authors acknowledge the computational resources used for the trajectory-optimization experiments. All figures reported in this manuscript were created by the authors.

Declarations

Funding

This research received no external funding.

Author contributions

Conceptualization: Hongxiang Luo and Yasheng Zhang. Methodology: Hongxiang Luo. Software: Hongxiang Luo and Zhongtao Zhang. Validation: Hongxiang Luo and Zhongtao Zhang. Formal analysis, investigation, data curation, visualization, and original-draft preparation: Hongxiang Luo. Resources and supervision: Hongxiang Luo and Yasheng Zhang. Writing–review and editing: Hongxiang Luo, Zhongtao Zhang, Yasheng Zhang, Xuefeng Tao, Wenhua Cheng, and Yuan Zeng. All authors read and approved the final manuscript and accept responsibility for its content.

Data availability

The numerical data supporting the findings of this study are available from the corresponding author upon reasonable request.

Code availability

The MATLAB scripts used to generate the numerical results are available from the corresponding author upon reasonable request.

Competing interests

The authors declare no competing interests.

References

[1] NASA. Gateway. https://www.nasa.gov/mission/gateway/ (2026).

[2] NASA. CAPSTONE. https://www.nasa.gov/mission/capstone/ (2026).

[3] Whitley, R. & Martinez, R. Options for staging orbits in cislunar space. In *2016 IEEE Aerospace Conference* 1–9 (2016). https://doi.org/10.1109/AERO.2016.7500635.

[4] Szebehely, V. *Theory of Orbits: The Restricted Problem of Three Bodies* (Academic Press, 1967).

[5] Pontryagin, L. S., Boltyanskii, V. G., Gamkrelidze, R. V. & Mishchenko, E. F. *The Mathematical Theory of Optimal Processes* (Interscience, 1962).

[6] Lawden, D. F. *Optimal Trajectories for Space Navigation* (Butterworths, 1963).

[7] Benson, D. A., Huntington, G. T., Thorvaldsen, T. P. & Rao, A. V. Direct trajectory optimization and costate estimation via an orthogonal collocation method. *J. Guid. Control Dyn.* **29**, 1435–1440 (2006). https://doi.org/10.2514/1.20478.

[8] Patterson, M. A. & Rao, A. V. GPOPS-II: A MATLAB software for solving multiple-phase optimal control problems using hp-adaptive Gaussian quadrature collocation methods and sparse nonlinear programming. *ACM Trans. Math. Softw.* **41**, 1–37 (2014). https://doi.org/10.1145/2558904.

[9] Haberkorn, T., Martinon, P. & Gergaud, J. Low-thrust minimum-fuel orbital transfer: A homotopic approach. *J. Guid. Control Dyn.* **27**, 1046–1060 (2004). https://doi.org/10.2514/1.4022.

[10] Gergaud, J. & Haberkorn, T. Homotopy method for minimum consumption orbit transfer problem. *ESAIM Control Optim. Calc. Var.* **12**, 294–310 (2006). https://doi.org/10.1051/cocv:2005036.

[11] Malyuta, D., Yu, Y., Elango, P. & Açıkmese, B. Advances in trajectory optimization for space vehicle control. *Annu. Rev. Control* **52**, 282–315 (2021). https://doi.org/10.1016/j.arcontrol.2021.04.013.

[12] Morante, D., Sanjurjo Rivo, M. & Soler, M. A survey on low-thrust trajectory optimization approaches. *Aerospace* **8**, 88 (2021). https://doi.org/10.3390/aerospace8030088.

[13] Ayyanathan, P. J. & Taheri, E. Mapped adjoint control transformation method for low-thrust trajectory design. *Acta Astronaut.* **193**, 418–431 (2022). https://doi.org/10.1016/j.actaastro.2021.12.019.

[14] Du, C., Wu, K., Starinova, O. L. & Liu, Y. Two trajectory configurations for the low-thrust transfer between northern and southern halo orbits in the Earth–Moon system. *Adv. Space Res.* **72**, 4093–4105 (2023). https://doi.org/10.1016/j.asr.2023.08.007.

[15] Oshima, K. Regularized direct method for low-thrust trajectory optimization: Minimum-fuel transfer between cislunar periodic orbits. *Adv. Space Res.* **72**, 2051–2063 (2023). https://doi.org/10.1016/j.asr.2023.05.055.

[16] Hecht, G. R. & Botta, E. M. Particle swarm optimization-based co-state initialization for low-thrust minimum-fuel trajectory optimization. *Acta Astronaut.* **211**, 416–430 (2023). https://doi.org/10.1016/j.actaastro.2023.06.021.

[17] Nurre, N. P. & Taheri, E. Duty-cycle-aware low-thrust trajectory optimization using embedded homotopy. *Acta Astronaut.* **212**, 630–642 (2023). https://doi.org/10.1016/j.actaastro.2023.08.022.

[18] Ottesen, D. & Russell, R. P. Direct-to-indirect mapping for optimal low-thrust trajectories. *Astrodynamics* **8**, 27–46 (2024). https://doi.org/10.1007/s42064-023-0164-6.

[19] Huang, Y., Zhang, L. & Zhang, X. A modified robust homotopic method for the low-thrust fuel-optimal orbital control problem. *Aerospace* **11**, 766 (2024). https://doi.org/10.3390/aerospace11090766.

[20] Du, C., Song, L., Zhang, J. & Liu, Y. A novel calculation method for low-thrust transfer trajectories in the Earth–Moon restricted three-body problem. *Aerosp. Sci. Technol.* **147**, 109048 (2024). https://doi.org/10.1016/j.ast.2024.109048.

[21] Wang, D., Ye, D. & Sun, Z. Shape-based method for low-thrust transfers between periodic orbits in cislunar space. *Acta Astronaut.* **219**, 996–1006 (2024). https://doi.org/10.1016/j.actaastro.2024.03.016.

[22] Fu, L., Chen, S., Guan, X. & Liu, Y. Mapping analytical costate estimation method based smoothing homotopy technique for low-thrust trajectory optimization. *Adv. Space Res.* **76**, 5199–5218 (2025). https://doi.org/10.1016/j.asr.2025.07.086.